Single-frame measurement of complex laser pulses tens of picoseconds long using pulse-front tilt in cross-correlation frequency-resolved optical gating

Tsz Chun Wong* and Rick Trebino

School of Physics, Georgia Institute of Technology, 837 State Street, Atlanta, Georgia 30332, USA
*Corresponding author: jeff.wong@gatech.edu

We demonstrate the use of pulse-front tilt (PFT) in cross-correlation frequency-resolved optical gating (XFROG) implemented in polarization-gate geometry to measure arbitrary complex ultrashort pulses tens of picoseconds long on a single-camera frame with the potential for a single-shot measurement. The PFT is generated by a diffraction grating. We measured chirped double pulses separated by 4.7 and 24 ps with fine details and accurately retrieved them using the standard XFROG retrieval algorithm. The temporal range of our device is 28 ps, an order of magnitude longer than available from standard single-shot FROG devices without PFT.   © 2013 Optical Society of America

OCIS codes: (320.0320) Ultrafast optics; (320.7100) Ultrafast measurements.
http://dx.doi.org/10.1364/JOSAB.30.002781

1. INTRODUCTION

In the past few decades, the pulse durations of ultrafast lasers have fallen from nanosecond (ns) lengths produced by Q switching [1] to attosecond (as) lengths from high-harmonic generation [2,3]. Pulse-*measurement* technology, however, has traditionally lagged behind pulse-generation technology. Autocorrelation gave a rough measure of pulse lengths of picosecond (ps) and eventually femtosecond (fs) pulses from the 1960s until the early 1990s. In 1991, the invention of frequency-resolved optical gating (FROG) [4] provided the complete temporal intensity and phase for an arbitrary fs pulse. Numerous variations of FROG have been developed since then to solve a variety of measurement challenges. Its simplified, inherently single-shot version, GRENOUILLE, measures relatively simple pulses [5,6]. More complex pulses with time–bandwidth products (TBPs) as high as 100 can also be measured using FROG [4,7], but, with a well-characterized reference pulse, cross-correlation frequency-resolved optical gating (XFROG) [8–12] has measured pulses with TBPs as large as several thousand and several ps long. When a previously measured reference pulse is not available, double-blind FROG can be used to measure two unknown pulses simultaneously [13,14]. All these FROG variations, as well as other techniques, focus mainly on the fs regime, largely because fs-long pulses were the shortest and hence most exciting pulses at the time these techniques were developed.

While fs-long pulses are now generally very accurately measured, much less attention has been devoted to the measurement of many-ps-long pulses for the above reason and also, interestingly, because they are actually *more* difficult to measure than fs pulses due to the much larger delays and higher spectral resolution required to measure them. But ps lasers remain widely used in scientific research, such as biological system imaging and control [15,16], the study of laser-induced effects and damage in materials [17–22], material processing [23–27], and ultrafast fluorescence spectroscopy [28]. They also find applications in industry because they are easier to work with than fs pulses, which broaden unacceptably in propagating through materials. For example, ophthalmological applications range from corneal ablation [29,30] to intraocular photodisruption [31,32] to laser *in situ* keratomileusis (LASIK) [33]. Other health-care applications from hair and tattoo removal [34–36] to cancer treatments to dental drilling [37–39] use ps pulses. And they find use in material processing applications from glass cutting [40] to circuit-board etching [41] to micromachining [42–44]. The accuracy and efficiency of all of these applications depend heavily on the ability to measure the laser pulses. Thus a technique that can completely characterize many-ps-long pulses would be beneficial, not only to the scientific community, but also to the industrial and medical communities.

The main approach for measuring many-ps-long pulses has long been multishot intensity autocorrelation using a delay-scanning stage and such optical nonlinearities as second-harmonic generation (SHG) [45–47], two-photon photoconductivity [48,49], two-photon fluorescence [50,51], and high-order effects [52,53]. Multishot interferometric autocorrelation [54,55], also using a scanning delay stage, has also been used. Longer (few-hundred ps) pulses are routinely measured using fast detectors and ultrahigh-bandwidth oscilloscopes. These devices achieve single-shot operation, but they are extremely expensive and only yield the intensity, and not the phase. Modern pulse-measurement techniques like FROG can be naturally extended to measure

many-ps-long pulses using a many-centimeter-long delay line, but any such approach is also necessarily a *multishot* measurement, which is undesirable in many circumstances, especially when fluctuations exist in the laser system [56,57].

Single-shot measurements of fs pulses are routinely achieved by crossing two pulses in the nonlinear medium at a large angle, which maps delay onto transverse position, yielding up to a few ps of relative delay. And there is actually a well-known and simple method for performing single-shot measurements of many-ps-long pulses, and it involves the use of pulse-front tilt (PFT). Crossing two *oppositely tilted* pulses in the nonlinear medium can yield tens of ps of relative delay. In 1981, Wyatt and Marinero first demonstrated the use of a diffraction grating to generate significant PFT for single-shot autocorrelation measurement with a temporal range of up to 80 ps [58]. More recently, Bowlan and Trebino extended the idea to even larger delays using an etalon to measure ns-long pulses with SHG FROG on a single shot [59]. However, these ideas have not yet been applied to the complete intensity-and-phase measurement of many-ps-long pulses, especially complex ones.

Here, we report the use of PFT in polarization-gating (PG) XFROG to measure pulses up to 28 ps long. Our motivation for this work is the future single-shot intensity-and-phase measurement of supercontinuum—an important unsolved problem. In such a measurement, significant PFT in the supercontinuum is undesirable, however, due to its extreme spectral width and the resulting potentially deleterious effects that the angular dispersion that necessarily accompanies PFT could have on its beam. As a result, we only tilt a spectrally much narrower reference pulse and use an XFROG (spectrally resolved cross-correlation) approach in which the reference pulse is used to measure the unknown (eventually supercontinuum) pulse. Also, the PG geometry is ideal for this application because it is automatically phase matched for all wavelengths and angles, entirely eliminating any problems associated with these issues.

2. ISSUE IN SINGLE-SHOT MANY-PS PULSE MEASUREMENT

Single-shot FROG measurements of fs-long pulses are routinely accomplished by crossing two beams at an angle of a few degrees inside the nonlinear medium. The nonlinear medium is then imaged onto a camera, which maps the temporal delay between the two beams to the transverse position of the camera. Increasing the crossing angle increases the temporal range of the device. However, this is not possible for measuring pulses longer than a few ps: to achieve a delay range of 30 ps, an internal crossing angle of 58°, corresponding to an external crossing angle of about 89° (assuming fused silica is the nonlinear medium) is required.

An additional important effect to consider when measuring complex pulses of any length is transverse geometrical smearing, in which a range of delays always occurs simultaneously due to the beam crossing angle, and which smears out fine temporal details in measurements using standard beam geometries in which the delay is varied using a moving mirror. But it is inherently not a problem in single-shot beam geometries because this effect is what actually allows the measurement to be single shot. Unfortunately, geometrical smearing can still wash out details in the trace due to variations in the delay

along the signal-beam direction [4]. This *longitudinal geometrical smearing* is identically zero in SHG-based FROGs and autocorrelators because the constant delay line in SHG precisely matches the signal-beam propagation direction. In the PG geometry, however, like all other non-SHG noncollinear geometries, longitudinal smearing is nonzero. The smearing depends not only on the thickness of the nonlinear medium, but also on the crossing angle. A detailed discussion of geometrical smearing can be found in [4]. But suffice it to say here that a large crossing angle of 58° inside a 250 μm thick nonlinear medium yields longitudinal smearing of 450 fs, which might be acceptable, but the smearing scales with thickness, and a thicker nonlinear medium is desirable for sensitivity considerations. So longitudinal geometrical smearing must be considered in any such measurements.

Another effect to be considered is beam size and the intensity drop-off away from the beam center. In practice, the usable temporal range of a PG XFROG setup is about 60% of the beam diameter. This effect is more pronounced in a third-order geometry, in which the signal is proportional to the cube of the input intensity. In addition, a large crossing angle reduces the interaction length between the two beams, which reduces the signal-to-noise ratio. A typical single-shot PG FROG setup (without PFT) involves a beam size of 8 mm and a crossing angle of ∼6° and yields a usable temporal range of 1.5 ps.

Here we demonstrate that a larger temporal range can be achieved in PG XFROG using PFT in the reference pulse generated by a diffraction grating in which the diffracted beam emerges along the normal to the grating surface, which, by simple path-length considerations, generates significant PFT. The grating surface is then *imaged* onto to the nonlinear medium to remove all other spatiotemporal distortions that generally exist after the pulse propagates with angular dispersion. PFT not only allows a greater delay range, but also yields reduced longitudinal smearing. In general, we find that the smearing is significantly less than that obtained by crossing beams without PFT, the precise factor depending on the actual configuration. This is because the temporal range in the PFT configuration is generated mainly by the tilted pulse front, so, in contrast to the untilted configuration, the crossing angle should be minimized to reduce the longitudinal smearing, reducing the smearing to almost zero. This can be seen easily from the two equations governing the temporal range, ΔT, and longitudinal smearing, δt, shown below:

$$\Delta T = \frac{d}{c} \tan(\alpha - \theta), \qquad (1)$$

$$\delta t = \frac{L}{c}\left(1 - \frac{\cos \alpha}{\cos(\alpha - \theta)}\right), \qquad (2)$$

where d is the beam diameter, L is the thickness of the nonlinear medium, α is the PFT angle, and θ is the crossing angle. The formulas are derived from the schematic depicted in Fig. 1. The amount of longitudinal smearing is the time delay range that a single spatial position experiences. Ideally, one spatial position should correspond to only one time delay; however, after propagation by some distance, that particular spatial position corresponds to a different delay. Consider the case in Fig. 1(b), in which the center of the beam corresponds
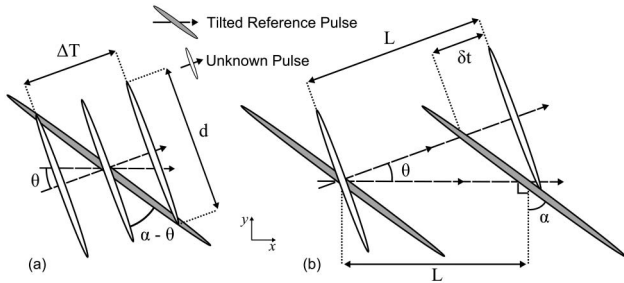
Fig. 1.   Illustration showing the calculation of (a) temporal range and (b) longitudinal smearing in PG XFROG with tilted pulse front in the reference pulse. The white and gray ellipses represent the untilted unknown pulse and the tilted reference pulse, respectively. The arrows represent the propagation directions of the two beams. Here, the tilted reference pulse propagates along the x axis, and the unknown pulse propagates at an angle, θ, with respect to the x axis. Using simple trigonometry, the temporal range of the measurement, ΔT, and the longitudinal smearing, δt, given in Eqs. (1) and (2) can be derived, where d is the beam diameter, L is the thickness of the nonlinear medium, and α is the PFT angle.

to the zero time delay at the entrance face of the nonlinear medium. As the two beams propagate at different directions, the center of the beam varies its delay. By the time the beams exit the nonlinear medium, the center of the beam will contain information from a range of delays. This range of delay, δt, is the longitudinal smearing of the system. This effect is discussed in great detail in [4]. It is clear from Eq. (2) that the longitudinal smearing will be zero for any value of α when θ is zero. Even though $\theta = 0$ gives a highly desirable zero longitudinal smearing configuration, it is not practical due to the presence of other optics, which sets the lower limit of the crossing angle and hence also of the longitudinal geometrical smearing.

3. EXPERIMENTAL SETUP

The experimental schematic of our ps PG XFROG is shown in Fig. 2. We begin with a 70 fs pulse with a center wavelength of 800 nm at a 1 kHz repetition rate from a Ti:sapphire regenerative amplifier (Coherent Legend Elite). The beam with
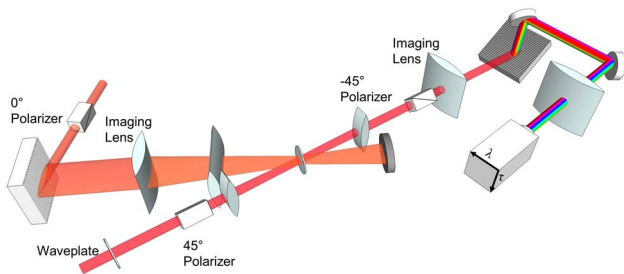

Fig. 2.   Schematic of our ps XFROG, implemented with a polarization-gate geometry. The unknown pulse to be measured is shown in red, and the tilted reference pulse is in orange. A diffraction grating with 1200 lines/mm was used generate the PFT. The first-order diffraction, propagating parallel to the normal of the grating, was used as the reference pulse. The surface of the diffraction grating was imaged onto the nonlinear medium to eliminate all the spatiotemporal distortions except PFT. The two beams crossed at an angle inside the nonlinear medium, mapping temporal delay between the two beams to the transverse position for single-shot measurement. The nonlinear medium was imaged onto the camera to map delay onto the transverse position of camera. The signal was filtered by the crossed polarizers and spectrally resolved to generate an XFROG trace.

diameter, d, of 8 mm is split into two using an 80/20 beam splitter. The higher-power pulse served as the reference pulse and the low-power one served as the unknown pulse. A fused silica parallel plate with thickness, L, of 250 μm was used as the nonlinear medium.

The reference pulse, shown in orange, first passed through a polarizer at 0° to increase the polarization purity before reaching a 1200 lines/mm diffraction grating. This pulse impinged on the grating at a grazing incidence angle so that the first-order diffraction was diffracted approximately along the normal of the grating surface. This is useful for the imaging condition from the grating surface to the nonlinear medium to be satisfied, as the depth of field is only about 5 mm. The zeroth-order diffraction from the grating was sent to a GRENOUILLE (Swamp Optics, model 8-20) for characterization (not shown in the schematic). Imaging was achieved using a 200 mm cylindrical imaging lens placed 700 mm away from the grating surface; it imaged the grating surface with a magnification of 0.4 onto the nonlinear medium. A 150 mm focusing lens was used to focus the beam in the vertical dimension. The unknown pulse (to be measured), shown in red, passed through a half-wave plate, which rotated the polarization by 45°, and then a pair of crossed polarizers at ±45°. A pair of lenses, each with a focal length of 100 mm, was used for focusing and collimating in the vertical dimension.

Like other single-shot FROG techniques, the two beams crossed at an angle in the nonlinear medium, and the nonlinear medium was imaged onto the camera to map delay to the transverse position. When the reference and unknown pulses overlapped spatially and temporally inside the nonlinear medium, polarization rotation occurred due to the induced birefringence, as in other PG arrangements. The rotated polarization in the unknown pulse passed through the crossed polarizer and served as the signal beam. The signal was spectrally resolved using an inexpensive homemade spectrometer consisting of a 600 lines/mm grating and a cylindrical lens with 150 mm focal length. The measured XFROG trace (or spectrogram) was retrieved using the standard XFROG algorithm available on the Internet [60].

The PFT angle, α, was 73°, and the crossing angle, θ, was 11°. The calculated temporal range and longitudinal smearing of our experimental setup were ~50 ps and 315 fs, respectively, as calculated using Eqs. (1) and (2). However, due to the intensity drop-off at the edge of the beam, the temporal range that yielded highly accurate measurement was about 28 ps. The temporal resolution of the system was limited by the longitudinal smearing of 315 fs. In general, this implies that any temporal structure shorter than 300 fs is washed out due to the lack of temporal resolution in the measured trace. However, *spectral* structure in the measured XFROG trace can allow the recovery of this otherwise lost information. The experimental apparatus was set up for single-shot measurement, but in the case of weak signals, one can increase the exposure time of the camera to integrate over multiple shots and perform multishot, but "single-camera-frame," measurements.

4. MEASUREMENTS

We first tested our ps PG XFROG setup using a known reference pulse with a FWHM of 70 fs to measure a double pulse

generated by a Michelson interferometer with separation of ~4.7 ps and chirped by 14 cm of SF11. The energies of the reference pulse and the unknown pulse were 720 and 45 μJ, respectively. Due to the beam splitting and chirping, the signal pulse was too weak for true single-shot measurement, so the measured XFROG trace averaged over five shots on a single-camera frame. A single-shot measurement could be performed with increased energy in either the reference pulse or the unknown pulse.

The measured and retrieved FROG traces (2048-by-2048 array), with G-error (the rms difference between the measured and retrieved FROG trace [4]) of 1.37%, are shown in Figs. 3(a) and 3(b). The temporal and spectral intensity and phase are shown in Figs. 3(c) and 3(d). The retrieved double-pulse separation was 4770 fs with FWHM of 1700 fs. To verify our measurement, we blocked one of arm of the Michelson and measured the unknown pulse before it passed through 14 cm of SF11 by using GRENOUILLE. The retrieved unknown pulse from GRENOUILLE was numerically propagated through 14 cm of SF11 yielding a FWHM of 1716 fs, in excellent agreement with the result from ps PG XFROG. The spectrum of the double pulse, shown in black, was measured by a spectrometer (Ocean Optics, HR4000). The double-pulse separation was calculated to be 4736 fs using the spectral fringe spacing, which agrees well with our retrieval. The retrieved pulse had a TBP of ~89. The discrepancies between the retrieved and the calculated pulse separation and FWHM are about 1%.

A 24 ps separated double pulse with TBP of ~263 was retrieved with G-error of 1.73%. The measured and retrieved traces are shown in Fig. 4. The retrieved separation and FWHM were 24,400 and 1780 fs, respectively. The calculated FWHM is 1772 fs, in good agreement with the retrieval. The spectrometer lacked the spectral resolution to resolve the fine spectral fringes (see the black line shown in the spectral measurement of Fig. 4). Thus, instead of using the spectral fringes, the separation was calculated from the position of the variable arm of the Michelson interferometer. The calculated separation was 24,469 fs, within 1% of the retrieved value.
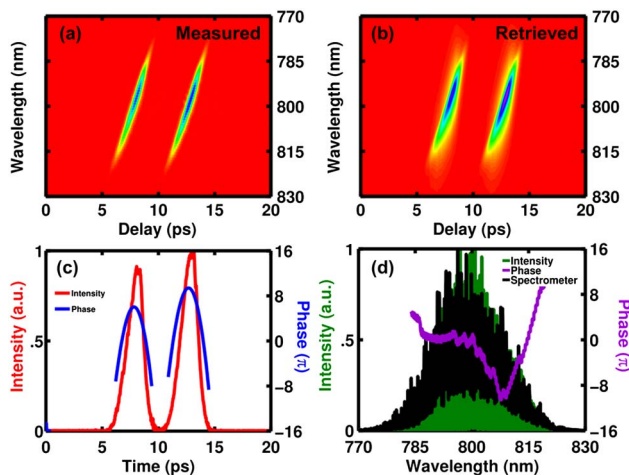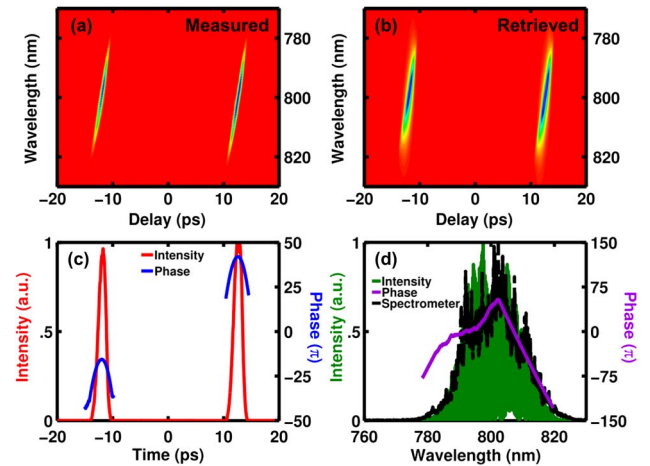

Fig. 4. (a) Measured and (b) retrieved XFROG traces of a double pulse with pulse separation of ~24 ps with G-error of 1.73%. (c) Retrieved temporal and (d) spectral intensity and phase. The black solid line represents the spectrum measured by a spectrometer. The retrieved pulse separation was 24,400 fs, and the FWHM was 1780 fs.

The G-error in our retrieval is relatively high for XFROG traces with array size of 2048. There are several factors that contribute to the high G-error. First, some of the polarizer leakage added to the measured trace coherently as a background. The leakage is a combination of imperfections in the polarizers and depolarization after the beam passed through the focusing and collimating lenses. This leakage background was about 8% of the peak signal strength. Since the background added partially coherently, it cannot be completely removed from the signal. Second, the signal near the wings of the trace was weak, and it falls to the background noise level, which was removed by somewhat overzealous background subtraction (confirmed by the unusually low-noise and nearly zero trace background). The XFROG retrieval algorithm is capable of recognizing these nonphysical flaws in the measured trace and fills in the missing details to produce the retrieved trace associated with the correct pulse. However, the resulting G-error will be relatively high due to the mismatch between the measured and retrieved traces. Finally, the measurements were made by averaging five shots from a regenerative amplifier, and the measurement could be affected by the instability of this laser [56,57].

There is also a discrepancy between the measured and retrieved spectra. The retrieved spectrum actually has higher spectral resolution than the experimental apparatus. In fact, the retrieval algorithm takes advantage of the redundancy in the N-by-N FROG trace to reproduce the detailed features of the pulse that are not measured by the apparatus [12]. Even though the home-brew spectrometer in ps PG XFROG lacks the spectral resolution to measure the fine spectral fringes, the retrieval algorithm is capable of reproducing the correct spectral fringes. Indeed, the spectral fringes are too fine to be shown in the plots, and become a solid green area under the curve.

The nonlinear medium used in the experiment was fused silica, which does not have a particularly high third-order nonlinear susceptibility. To improve the signal-to-noise ratio, one could increase the thickness of the medium (this will, however, increase the longitudinal smearing) or replace the nonlinear medium with another material with higher third-order

Fig. 3. (a) Measured and (b) retrieved XFROG traces of a double pulse with pulse separation of ~4.7 ps with G-error of 1.37%. (c) Retrieved temporal and (d) spectral intensity and phase. The black solid line represents the spectrum measured by a spectrometer. The retrieved pulse separation was 4770 fs, and the FWHM was 1700 fs.

nonlinearity, such as BK7. The resulting G-error would be reduced and better signal-to-noise ratio achieved. This could also allow a single-shot measurement, which would eliminate any effects due to instability. A single-shot measurement is particularly important in the case of supercontinuum, as it experiences significant shot-to-shot fluctuations. A typical supercontinuum has a spectrum of more than 100 nm and spans more than 10 ps in time. In order to measure it on a single shot, the device should use a reference pulse with more pulse energy or a thicker nonlinear medium or one with greater nonlinearity. We estimate that an optimized device could measure a supercontinuum with pulse energy of 100 nJ. Unfortunately, geometrical smearing, which is an issue in PG devices, could wash out the fine temporal structure in the trace of such a complex pulse as continuum, and we are currently addressing this issue. It will be the subject of a future publication.

5. CONCLUSION

We demonstrated the use of PFT in PG XFROG to increase the temporal range from ~1 to 28 ps with a temporal resolution of 300 fs. This is, to the best of our knowledge, the first demonstration of a single-frame configuration for a ps FROG device. By choosing a proper combination of groove density of the grating and magnification of the imaging system, one can control the desired temporal range of the device. This idea could be scaled up to perform single-shot measurement of few-hundred-ps-long pulses easily. The robust XFROG retrieval algorithm is able to retrieve missing details of the pulse due to both low spectral resolution and low signal-to-noise ratio. This device is an excellent candidate to perform single-shot measurement of supercontinuum generation, which is typically ~10 ps long with a spectrum of more than 100 nm.

ACKNOWLEDGMENTS

REFERENCES

1. F. J. McClung and R. W. Hellwarth, "Giant optical pulsations from ruby," J. Appl. Phys. **33**, 828–829 (1962).
2. E. Goulielmakis, M. Schultze, M. Hofstetter, V. S. Yakovlev, J. Gagnon, M. Uiberacker, A. L. Aquila, E. M. Gullikson, D. T. Attwood, R. Kienberger, F. Krausz, and U. Kleineberg, "Single-cycle nonlinear optics," Science **320**, 1614–1617 (2008).
3. K. Zhao, Q. Zhang, M. Chini, Y. Wu, X. Wang, and Z. Chang, "Tailoring a 67 attosecond pulse through advantageous phase-mismatch," Opt. Lett. **37**, 3891–3893 (2012).
4. R. Trebino, *Frequency-Resolved Optical Gating: The Measurement of Ultrashort Laser Pulses* (Kluwer Academic, 2002).
5. S. Akturk, M. Kimmel, P. O'Shea, and R. Trebino, "Extremely simple device for measuring 20-fs pulses," Opt. Lett. **29**, 1025–1027 (2004).
6. P. O'Shea, M. Kimmel, X. Gu, and R. Trebino, "Highly simplified device for ultrashort-pulse measurement," Opt. Lett. **26**, 932–934 (2001).
7. L. Xu, E. Zeek, and R. Trebino, "Simulations of frequency-resolved optical gating for measuring very complex pulses," J. Opt. Soc. Am. B **25**, A70–A80 (2008).
8. S. Linden, H. Giessen, and J. Kuhl, "XFROG-a new method for amplitude and phase characterization of weak ultrashort pulses," Phys. Status Solidi B **206**, 119–124 (1998).
9. A. Yabushita, T. Fuji, and T. Kobayashi, "SHG FROG and XFROG methods for phase/intensity characterization of pulses propagated through an absorptive optical medium," Opt. Commun. **198**, 227–232 (2001).
10. Q. Cao, X. Gu, E. Zeek, M. Kimmel, R. Trebino, J. Dudley, and R. S. Windeler, "Measurement of the intensity and phase of supercontinuum from an 8-mm-long microstructure fiber," Appl. Phys. B **77**, 239–244 (2003).
11. D. Lee, P. Gabolde, and R. Trebino, "Toward single-shot measurement of broadband ultrafast continuum," J. Opt. Soc. Am. B **25**, A25–A33 (2008).
12. X. Gu, L. Xu, M. Kimmel, E. Zeek, P. O'Shea, A. P. Shreenath, R. Trebino, and R. S. Windeler, "Frequency-resolved optical gating and single-shot spectral measurements reveal fine structure in microstructure-fiber continuum," Opt. Lett. **27**, 1174–1176 (2002).
13. T. C. Wong, J. Ratner, V. Chauhan, J. Cohen, P. M. Vaughan, L. Xu, A. Consoli, and R. Trebino, "Simultaneously measuring two ultrashort laser pulses on a single-shot using double-blind frequency-resolved optical gating," J. Opt. Soc. Am. B **29**, 1237–1244 (2012).
14. T. C. Wong, J. Ratner, and R. Trebino, "Simultaneous measurement of two different-color ultrashort pulses on a single shot," J. Opt. Soc. Am. B **29**, 1889–1893 (2012).
15. R. Kawakami, K. Sawada, A. Sato, T. Hibi, Y. Kozawa, S. Sato, H. Yokoyama, and T. Nemoto, "Visualizing hippocampal neurons with in vivo two-photon microscopy using a 1030 nm picosecond pulse laser," Sci. Rep. **3**, 1014 (2013).
16. G. Huettmann, B. Radt, J. Serbin, and R. Birngruber, "Inactivation of proteins by irradiation of gold nanoparticles with nano- and picosecond laser pulses," Proc. SPIE **5142**, 88–95 (2003).
17. P. L. Liu, R. Yen, N. Bloembergen, and R. T. Hodgson, "Picosecond laser-induced melting and resolidification morphology on Si," Appl. Phys. Lett. **34**, 864–866 (1979).
18. B. Zysset, J. G. Fujimoto, and T. F. Deutsch, "Time-resolved measurements of picosecond optical breakdown," Appl. Phys. B **48**, 139–147 (1989).
19. B. Zysset, J. G. Fujimoto, C. A. Puliafito, R. Birngruber, and T. F. Deutsch, "Picosecond optical breakdown: tissue effects and reduction of collateral damage," Lasers Surg. Med. **9**, 193–204 (1989).
20. B. C. Stuart, M. D. Feit, A. M. Rubenchik, B. W. Shore, and M. D. Perry, "Laser-induced damage in dielectrics with nanosecond to subpicosecond pulses," Phys. Rev. Lett. **74**, 2248–2251 (1995).
21. J. Noack and A. Vogel, "Laser-induced plasma formation in water at nanosecond to femtosecond time scales: calculation of thresholds, absorption coefficients, and energy density," IEEE J. Quantum Electron. **35**, 1156–1167 (1999).
22. B.-M. Kim, A. M. Komashko, A. M. Rubenchik, M. D. Feit, S. Reidt, L. B. D. Silva, and J. Eichler, "Interferometric analysis of ultrashort pulse laser-induced pressure waves in water," J. Appl. Phys. **94**, 709–715 (2003).
23. M. Malinauskas, P. Danilevičius, and S. Juodkazis, "Three-dimensional micro-/nano-structuring via direct write polymerization with picosecond laser pulses," Opt. Express **19**, 5602–5610 (2011).
24. B. Voisiat, M. Gedvilas, S. Indrišiūnas, and G. Račiukaitis, "Picosecond-laser 4-beam-interference ablation as a flexible tool for thin film microstructuring," Phys. Procedia **12**, 116–124 (2011).
25. T. Jiang, J. Koch, C. Unger, E. Fadeeva, A. Koroleva, Q. Zhao, and B. Chichkov, "Ultrashort picosecond laser processing of micro-molds for fabricating plastic parts with superhydrophobic surfaces," Appl. Phys. A **108**, 863–869 (2012).
26. R. Moser, M. Kunzer, C. Goßler, R. Schmidt, K. Köhler, W. Pletschen, U. T. Schwarz, and J. Wagner, "Laser processing of GaN-based LEDs with ultraviolet picosecond laser pulses," Proc. SPIE **8433**, 84330Q (2012).
27. R. Intartaglia, G. Das, K. Bagga, A. Gopalakrishnan, A. Genovese, M. Povia, E. Di Fabrizio, R. Cingolani, A. Diaspro, and F. Brandi, "Laser synthesis of ligand-free bimetallic nanoparticles for plasmonic applications," Phys. Chem. Chem. Phys. **15**, 3075–3082 (2013).
28. Y. Pu, W. Wang, R. B. Dorshow, B. B. Das, and R. R. Alfano, "Review of ultrafast fluorescence polarization spectroscopy [Invited]," Appl. Opt. **52**, 917–929 (2013).

29. D. Stern, R. W. Schoenlein, C. A. Puliafito, E. T. Dobi, R. Birngruber, and J. G. Fujimoto, "Corneal ablation by nanosecond, picosecond, and femtosecond lasers at 532 and 625 nm," Arch. Ophthalmol. **107**, 587–592 (1989).

30. X.-H. Hu and T. Juhasz, "Study of corneal ablation with picosecond laser pulses at 211 nm and 263 nm," Lasers Surg. Med. **18**, 373–380 (1996).

31. A. Vogel, S. Busch, K. Jungnickel, and R. Birngruber, "Mechanisms of intraocular photodisruption with picosecond and nanosecond laser pulses," Lasers Surg. Med. **15**, 32–43 (1994).

32. J. M. Krauss and C. A. Puliafito, "Lasers in ophthalmology," Lasers Surg. Med. **17**, 102–159 (1995).

33. R. R. Krueger, T. Juhasz, A. Gualano, and V. Marchi, "The picosecond laser for nonmechanical laser in situ keratomileusis," J. Refract. Surg. **14**, 467–469 (1998).

34. E. F. Bernstein, "Laser tattoo removal," Semin. Plast. Surg. **21**, 175–192 (2007).

35. N. Saedi, A. Metelitsa, K. Petrell, K. A. Arndt, and J. S. Dover, "Treatment of tattoos with a picosecond alexandrite laser: a prospective trial," Arch. Dermatol. **148**, 1360–1363 (2012).

36. N. I. Tankovich, A. M. Hunter, and K. Y. Tang, "Hair removal device and method," U.S. patent 6,267,771 (July 31, 2001).

37. M. H. Niemz, "Cavity preparation with the Nd:YLF picosecond laser," J. Dent. Res. **74**, 1194–1199 (1995).

38. A. A. Serafetinides, M. G. Khabbaz, M. I. Makropoulou, and A. K. Kar, "Picosecond laser ablation of dentine in endodontics," Lasers Med. Sci. **14**, 168–174 (1999).

39. M. S. Bello-Silva, M. Wehner, C. P. Eduardo, F. Lampert, R. Poprawe, M. Hermans, and M. Esteves-Oliveira, "Precise ablation of dental hard tissues with ultra-short pulsed lasers. Preliminary exploratory investigation on adequate laser parameters," Lasers Med. Sci. **28**, 171–184 (2013).

40. M. B. Strigin and A. N. Chudinov, "Cutting of glass by picosecond laser radiation," Opt. Commun. **106**, 223–226 (1994).

41. D. Shin, J. Lee, H. Sohn, J. Noh, and B. Paik, "A FPCB cutting process using a picosecond laser," J. Laser Micro/Nanoeng. **5**, 48–52 (2010).

42. B. N. Chichkov, C. Momma, S. Nolte, F. Alvensleben, and A. Tünnermann, "Femtosecond, picosecond and nanosecond laser ablation of solids," Appl. Phys. A **63**, 109–115 (1996).

43. N. N. Nedialkov, S. E. Imamova, and P. A. Atanasov, "Ablation of metals by ultrashort laser pulses," J. Phys. D **37**, 638–643 (2004).

44. J. Cheng, C.-S. Liu, S. Shang, D. Liu, W. Perrie, G. Dearden, and K. Watkins, "A review of ultrafast laser materials micromachining," Opt. Laser Technol. **46**, 88–102 (2013).

45. J. A. Armstrong, "Measurement of picosecond laser pulse widths," Appl. Phys. Lett. **10**, 16–18 (1967).

46. H. P. Weber and H. G. Danielmeyer, "Multimode effects in intensity correlation measurements," Phys. Rev. A **2**, 2074–2079 (1970).

47. E. P. Ippen, C. V. Shank, and A. Dienes, "Passive mode locking of the cw dye laser," Appl. Phys. Lett. **21**, 348–350 (1972).

48. C. Lee and S. Jayaraman, "Measurement of ultrashort optical pulses by two-photon photoconductivity techniques," Optoelectronics **6**, 115–120 (1974).

49. Y. Takagi, T. Kobayashi, K. Yoshihara, and S. Imamura, "Multiple- and single-shot autocorrelator based on two-photon conductivity in semiconductors," Opt. Lett. **17**, 658–660 (1992).

50. P. Sperber and A. Penzkofer, "Pulse-shape determination of intracavity compressed picosecond pulses by two-photon fluorescence analysis," Opt. Quantum Electron. **18**, 145–154 (1986).

51. J. A. Giordmaine, P. M. Rentzepis, S. L. Shapiro, and K. W. Wecht, "Two-photon excitation of fluorescence by picosecond light pulses," Appl. Phys. Lett. **11**, 216–218 (1967).

52. S. Luan, M. H. R. Hutchinson, R. A. Smith, and F. Zhou, "High dynamic range third-order correlation measurement of picosecond laser pulse shapes," Meas. Sci. Technol. **4**, 1426–1429 (1993).

53. H. P. Weber and R. Dändliker, "Method for measurement the shape asymmetry of picosecond light pulses," Phys. Lett. A **28**, 77–78 (1968).

54. T. Mindl, P. Hefferle, S. Schneider, and F. Dörr, "Characterisation of a train of subpicosecond laser pulses by fringe resolved autocorrelation measurements," Appl. Phys. B **31**, 201–207 (1983).

55. P. Yeh, "Autocorrelation of ultrashort optical pulses using polarization interferometry," Opt. Lett. **8**, 330–332 (1983).

56. J. Ratner, G. Steinmeyer, T. C. Wong, R. Bartels, and R. Trebino, "Coherent artifact in modern pulse measurements," Opt. Lett. **37**, 2874–2876 (2012).

57. M. Rhodes, G. Steinmeyer, J. Ratner, and R. Trebino, "Pulse-shape instabilities and their measurement," Laser Photon. Rev. **7**, 557–565 (2013).

58. R. Wyatt and E. E. Marinero, "Versatile single-shot background-free pulse duration measurement technique, for pulses of sub-nanosecond to picosecond duration," Appl. Phys. **25**, 297–301 (1981).

59. P. Bowlan and R. Trebino, "Complete single-shot measurement of arbitrary nanosecond laser pulses in time," Opt. Express **19**, 1367–1377 (2011).

60. R. Trebino, "Ultrafast Optics Group in Georgia Institute of Technology," http://frog.gatech.edu/.